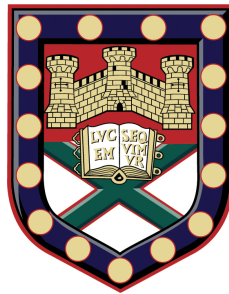


# Semiconductor surface plasmons: a route to terahertz waveguides and sensors



Edmund Keith Stone

School of Physics

University of Exeter

A thesis submitted for the degree of

*Doctor of Philosophy*

March 2012

# Semiconductor surface plasmons: a route to terahertz waveguides and sensors

Submitted by Edmund Keith Stone to the University of Exeter as a thesis for  
the degree of Doctor of Philosophy in Physics  
2012

This thesis is available for Library use on the understanding that it is copyright material and that no quotation from the thesis may be published without proper acknowledgement.

I certify that all material in this thesis which is not my own work has been identified and that no material has previously been submitted and approved for the award of a degree by this or any other University.

Edmund Keith Stone  
2012

I would like to dedicate this thesis to Phyllis Mary Hamblen my loving gran who passed away during my second year.

## Acknowledgements

During my time at Exeter many people have helped me, kept me sane and fed the insanity, all of which seem to be required for completing a PhD. To all those people, thank you. Lots are listed below, those who are not, I am sorry.

A special thank you must be said to my supervisor. Euan's enthusiasm for science is unshakable and affects all those around him. Even when the list of failed attempts appeared unending he was still positive. On a similar note, Professor Roy Sambles, thank you for suggesting my name to Euan and for your help in group meetings. Without my first summer project with you I'm not sure I would be writing a thesis currently. Tom Isaac, I am indebted to for teaching me all he knew about terahertz spectroscopy. Tom, the lock-in amplifier still only works if you catch it off guard when switching it on. During my time I have become more worried about the apparent sentience of some of our equipment.

I'd like to thank Professor Bill Barnes for many useful meetings whether it was 'back to basics,' terahertz or generation orientated. Always happy, and friendly with an insightful comment on the subject at hand. A great contributor to those early meetings was Baptiste, who along with Martin, Tim A, Tim T, John, Joe and Steph showed me just how interesting a PhD could be during my summer projects as an undergraduate. Others from the group who have moved on, Chris Burrows and James Parsons, you guys helped a lot with HFSS. James, your antics in the basement are still the topic of discussion, soon I feel the stuff of legend. Not forgetting Andy and George, your knowledge of the FIB and SEM was indispensable.

Matt L and Ian, as much as you might not like to admit it, you are both full of knowledge and happy to spread it about and help people, and between the unreproducible comments the discussions are nearly always useful. Two fellow terahertz spectroscopists, thanks for all your help Dmitry and Rostislav.

Matt B, Helen and Liz, since being undergrads together it's always been good to have a chat with you guys. Mel, thanks for helping me with maths when I hit a brick wall, even when the questions were ridiculously simple and I'd argued myself into a hole. It was always a pleasure helping you with your computer woes. Also, Mel, thanks for talking me through the panic, you'll be a great teacher! Celia, you should probably be mentioned several times in this section but tough. Thank you for all the talks, whether physics or unrelated, both at network and in uni you have always been a help and had

sensible words of advice. Tim ‘starkles’ Starkey, you are a unique individual, whether you’re fighting with HFSS or looking confused at experiments it’s always interesting. I’d like to thank the other members of the electromagnetics group who I’ve not named specifically and also the guys in other groups who’ve been good to talk to especially graphene about fabrication issues. On that note Pete Hale and Sam Hornett, two more of Euan’s students who have a wealth of knowledge and are happy to pass it on when it’s needed. And of course the workshop guys, Nick Cole especially, with Pete Cann, and Adam and Dave for finding me Helium when I was desperate to get some experiments done before the laser moved to its new home.

I did some demonstrating whilst doing my PhD, second year labs would not have been the same if it were not for Martin Smith, Lee Summers, and Steve Hubbard (and others mentioned in other places here), thank you guys for keeping me sane, especially you Lee, if the astro doesn’t work out you can always be a stand up.

There are several people who might be thinking they have been forgotten at this point, but a special mention has to go with those of us who spend our time in the basement of physics. Alfie, you are annoyingly funny, despite your similarities to Holmes. Steve, thanks for the discussions especially recently. Matt N, you missed the best times in the basement, sorry about that. Tom C, having you in the same office has been useful for someone to bounce ideas off, I hope I’ve helped you in the same way. Your proof reading of some of the chapters below was indispensable, thank you. Finally for physics, Caroline and Chris ‘CJ’ ‘Holmesey’ Holmes. I have spent most of the last 4 years with you guys. There is so much to say, the arguing, the word game, the list is pretty long. Thank you. Chris, you annoyed me greatly at some points, earthquakes, and using me as a drum kit are two things that spring to mind. But despite that you are a great friend and someone who I hope I do not lose contact with. Likewise Caroline, there are many things that could go here, none of which you would like me to write, I therefore will not. Just a heartfelt thank you, finish soon, we never did find the time to play a game of mini golf. I think that pretty much completes the list of people from physics, if I’ve missed you, sorry.

Outside physics there are a group of people who have helped keep me routed. Helped distract me when I’ve needed it and helped me get to this point in my life. My parents of course, they have always believed in me and supported me through everything I have done. If it was not for the way they have brought me up I do not know where I would be at this point. I should also thank my brother, Tris, for constantly suggesting I could wear things as a special hat. When Celia first met Tris, she was surprised as from when I talked about him she had assumed I was the older brother.

Some friends and influences from other places have also enabled me to get to this point. Friends from scouting, especially James and Matt, two of my oldest friends who

are always good for a distraction. And Mr Bushrod, a great inspiration, my first real science teacher when I was around 9 years old, he inspired me to find out how the world worked with some truly great teaching.

Lastly, Sarah, thank you for being honest and for being there, when discussing me day with you, you always listened and then pointed out you didn't know what I was talking about. And of course thank you for making me some amazing food, your cheesecake is just fantastic.

## Abstract

The terahertz regime has until recently been somewhat neglected due to the difficulty of generating and measuring terahertz radiation. Terahertz time domain spectroscopy has allowed for affordable and broadband probing of this frequency regime with phase sensitive measurements (chapter 3). This thesis aims to use this tool to add to the knowledge of the interactions between electromagnetic radiation and matter specifically in regard to plasmonics.

This thesis covers several distinct phenomena related to plasmonics at terahertz frequencies. The generation of terahertz radiation from metal nanoparticles is first described in chapter 4. It is shown that the field strength of the plasmon appears to relate to the strength of the generated field. It is also shown that the power dependence of the generated terahertz radiation is not consistent with the optical rectification description of this phenomenon. An alternative explanation is developed which appears more consistent with the observations. A simple model for the power dependence is derived and compared to the experimental results.

In chapter 5 the parameters that make good plasmonic materials are discussed. These parameters are used to assess the suitability of semiconductors for terahertz surface plasmon experiments. The Drude permittivity of InSb is measured here, leading to a discussion of terahertz particle plasmons in chapter 6. Finite element method modelling is used to show some merits of these over optical particle plasmons. This also includes a discussion of fabrication methods for arrays of these particles.

Finally, chapter 7 is a discussion of so called spoof surface plasmons. This includes some experimental work at microwave frequencies and an in depth analysis of open ended square hole arrays supported by model matching method modelling. Perfect endoscope effects are discussed and compared to superlensing. The thesis ends with a brief conclusions chapter where some of the ideas presented are brought together.

# Contents

Contents	vi
List of Figures	ix
Nomenclature	xviii
<b>1 Introduction</b>	<b>1</b>
<b>2 Theory</b>	<b>4</b>
2.1 Surface plasmons . . . . .	4
2.1.1 Dispersion relation of surface plasmons . . . . .	5
2.1.2 Surface plasmon polariton length scales . . . . .	8
2.1.3 Surface plasmon coupling methods . . . . .	11
2.2 Drude model . . . . .	12
2.3 Localised surface plasmons resonances . . . . .	15
2.3.1 Quasi-static approximation . . . . .	16
<b>3 Methods</b>	<b>19</b>
3.1 THz Spectroscopy . . . . .	19
3.1.1 Generation and detection . . . . .	23
3.1.2 Photodiode detectors . . . . .	29
3.2 Sample self adhesive support . . . . .	32
3.3 Optical spectra . . . . .	32
3.4 Finite Element Method Modelling . . . . .	33
3.4.1 Boundaries . . . . .	34
3.4.2 Incident wave solutions . . . . .	35
3.4.3 Eigenmode solutions . . . . .	35
3.4.4 Element meshing . . . . .	36
3.4.5 Uses . . . . .	36



<b>4</b>	<b>Nanoparticle plasmonic generation of terahertz radiation</b>	<b>37</b>
4.1	Samples . . . . .	38
4.2	Experimental set up . . . . .	41
4.3	Islandised films . . . . .	42
4.4	Nanosphere lithography arrays . . . . .	43
4.4.1	Thickness dependency . . . . .	44
4.4.1.1	Experimental results . . . . .	44
4.4.1.2	Numerical modelling . . . . .	45
4.4.2	Optical intensity dependency . . . . .	49
4.4.2.1	Simple model . . . . .	49
4.4.3	Angle dependence . . . . .	53
4.5	Conclusions and future proposals . . . . .	55
 <b>5</b>	 <b>Terahertz plasmonic materials</b>	 <b>56</b>
5.1	Drude parameters of optical plasmonic metals . . . . .	56
5.2	Drude model and semiconductors . . . . .	57
5.3	Terahertz plasmonic materials . . . . .	59
5.3.1	Measuring the Drude parameters . . . . .	59
5.3.2	Results . . . . .	61
5.3.2.1	Temperature dependence . . . . .	63
5.3.3	Comparison between semiconductors . . . . .	66
5.3.3.1	Modelling of gratings with different semiconductors . . . . .	68
5.3.4	Photoexcitation of InSb . . . . .	70
5.4	Conclusions . . . . .	76
 <b>6</b>	 <b>Terahertz particle plasmons</b>	 <b>77</b>
6.1	Fabrication . . . . .	80
6.1.1	Chemical wet etch . . . . .	80
6.1.2	Focused ion beam . . . . .	82
6.1.2.1	Post etching positioning . . . . .	83
6.1.2.2	Results . . . . .	85
6.1.3	Reactive ion etching and chromium masks . . . . .	86
6.2	Modelling results . . . . .	89
6.2.1	Particle pairs . . . . .	91
6.2.2	Varying sharpness . . . . .	92
6.2.3	Photomodulation . . . . .	97
6.3	Conclusions . . . . .	98

<b>7</b>	<b>Surface modes on open ended hole arrays</b>	<b>99</b>
7.0.1	Terahertz hole array measurement . . . . .	99
7.0.2	Motivations . . . . .	100
7.1	Theoretical formalism . . . . .	101
7.1.1	Modal matching approach . . . . .	101
7.1.2	Dispersion relations . . . . .	105
7.2	Results and discussion . . . . .	108
7.2.1	Measurement of surface mode dispersion . . . . .	108
7.2.2	Asymptotic frequencies and mode splitting . . . . .	112
7.3	Role of surface modes in hole array transmission . . . . .	114
7.3.1	Near field transmission of hole arrays . . . . .	114
7.3.2	Far field transmission of hole arrays . . . . .	117
7.4	Conclusions . . . . .	118
<b>8</b>	<b>Conclusions and future work</b>	<b>121</b>
8.1	Publications . . . . .	122
	<b>References</b>	<b>123</b>

# List of Figures

2.1	An incident p-polarised electromagnetic wave on the interface between two materials of different permittivity ( $\epsilon_d$ and $\epsilon_m$ ). . . . .	5
2.2	The dispersion relation for silver using a frequency dependent permittivity found from the Drude model . . . . .	8
2.3	The field confinement in the $z$ direction (normal to the surface) using a permittivity found using the Drude parameters of silver, (a) into the metal, and (b) into the dielectric, . . . . .	10
2.4	A schematic of the electric fields on the metal-dielectric interface for a surface plasmon polariton, the decay into the metal and dielectric are shown. For any moment in time the field must change direction along the surface as the surface charge wave is longitudinal. . . . .	11
2.5	Schematic diagram of the blade coupling method, a form of scattering coupling. . . . .	12
2.6	The path traced by an electron in a metal according to the Drude model. The electron undergoes many random scattering events resulting in a random walk. The solid line indicates the situation where there is no applied electric field and the dotted line the case when there is an applied electric field resulting in a drift velocity $v_d$ . . . . .	14
2.7	Example complex permittivity for metals in the optical regime, the solid lines represent the real part, and the dashed lines the imaginary part, for (a) silver and (b) aluminium, found using the Drude model. . . . .	15
3.1	Schematic of the focusing terahertz time domain spectrometer (THz-TDS) used in this project, the optical 800nm path is shown in red with the terahertz beam path shown in green. . . . .	20

3.2	(a) Schematic of the collimated terahertz time domain spectrometer (THz-TDS) in the transmission configuration used in this project, the optical 800nm path is shown in red with the terahertz beam path shown in green. (b) Schematic of the dry air box section of the collimated THz-TDS in the reflection configuration. . . . .	20
3.3	Example traces from a THz-TDS setup, (a) shows the time domain trace, whereas (b) shows the modulus of the complex frequency domain trace, also shown is the phase measured through the system. . . . .	23
3.4	An example photoconductive device, a bias voltage is applied across the antenna gap, when the incident optical pulse excites charge carriers their resultant acceleration results in an emitted pulse of terahertz radiation. . . . .	24
3.5	(a) The atomic structure of ZnTe . (b) The non-linear potential due to the assymmetric bond between the Zn and Te atoms. (c) the optical excitation pulse, with the induced polarisation in a very thin non-linear crystal, and the resulting terahertz pulse. . . . .	26
3.6	The dependence of the peak terahertz electric field on the fluence of the generating optical pulse for ZnTe (solid line), a non-linear optical rectification crystal, and a photoconductive antenna device (dotted line) with a 4 kV bias voltage. . . . .	28
3.7	The three considered circuit diagrams for balanced photodiodes. It should be noted that these diagrams are simplified containing only the most important components. (a) The situation where the diodes are unpowered and in parallel, their direct differential is then amplified. (b) Has two ‘pre-amps’, one for each of the diodes, the differential operation is conducted using an op-amp. (c) The pre-amps and differential amplifier are supplemented by a sample and hold stage to conduct the stretching, this is then amplified by a fourth op-amp. . . . .	31
3.8	The time domain transmission through 4 different self adhesive pressure sensitive films, shown with a free space transmission through the focussing THz spectrometer. . . . .	33
4.1	A schematic of the proposed generation method. . . . .	38
4.2	A scanning electron microscope image of an islandised film, with a mass-thickness of 12 nm, the narrow channels the film are clearly illustrated. . . . .	39
4.3	Nanosphere lithography process for fabricating nanoscale triangles. . . . .	40
4.4	A scanning electron microscope image of an array of triangles fabricated using 780 nm diameter spheres using nanosphere lithography with a deposited metal depth of 50 nm. . . . .	40

4.5	Optical extinction spectra for islandised films, and triangles fabricated by nanosphere lithography. . . . .	41
4.6	The peak terahertz intensity measured from islandised films with different mass-thickness. . . . .	42
4.7	(a) The time domain generated terahertz transmission from a 1 mm $\langle 110 \rangle$ ZnTe crystal (dashed line), and an array of triangular particles fabricated from nanosphere lithography using 780 nm (solid line) diameter spheres. (b) The frequency domain measurements of the generated terahertz signal, also shown (as the dotted line) is an array of triangles fabricated using and 390 nm diameter spheres. . . . .	43
4.8	Dependence of the peak generated terahertz intensity on the thickness of particles at normal incidence (solid line, filled circles) and an inclination angle (angle of incidence) of $40^\circ$ (dashed line, filled squares). The lines are shown to guide the eye. Both datasets are normalised to their respective peaks and the normal incidence measurements are around a factor of 10 smaller. The arrays was fabricated using 780 nm diameter spheres. . . . .	44
4.9	Characteristic field enhancement distributions for 40 nm thick curved particles in a rhombic unit cell calculated using finite element modelling, illuminated with a wavelength of 800 nm. (a) In cross-section, where the inset shows the probe position for the maximum field enhancement plots. (b) Looking in plan of the particles. . . . .	45
4.10	The dipolar plasmon resonance shown in the reflection spectra for different realistic modifications, modelled for triangles made from spheres with a diameter of 780 nm. . . . .	46
4.11	The realistic modifications made to the model. (a) The starting point with straight pointed triangles, (b) The difference between the straight sided and sloped particles, (c) The modification to the straight triangles to make the sides and points curved, and (d) showing the modification to the top (and bottom) edges to include a small amount of curvature. . . . .	47
4.12	Results of numerical modelling for curved triangular particles with rounded edges, (a) reflection spectra for different thicknesses, $h = 20, 30, 40, 50, 60,$ and 90 nm, the arrow shows the direction of increasing thickness and (b) the dependence of the peak field enhancements at 800 nm on the thickness of particles at normal incidence. . . . .	48

4.13	Dependence of generated terahertz fluence as a function of the intensity of the optical pulse incident onto the sample. ZnTe is shown as the circles and dashed line, with the squares and solid lines representing measurements of a NSL fabricated array, using spheres of diameter 780 nm and with a particle thickness of 50 nm. . . . .	50
4.14	Measured angle dependence of the generated terahertz intensity, from an array of 50 nm thick triangles fabricated using NSL with spheres of diameter 780 nm. Also shown are two predictions from (4.16) where $n_4 = 1$ (the dashed line) and $n_4 = 5$ (the dotted line). . . . .	54
5.1	Schematic of idealised conduction and valence electron bands for metals, semiconductors and insulators. The Fermi level is indicated by $E_F$ , up to which the electron states are filled. . . . .	58
5.2	Schematic of the transmission through a slab of material with refractive index $n_2$ . . . . .	60
5.3	(a) Real and (b) imaginary parts of the transmission of the two silicon samples in the frequency domain. Also shown is the (c) real and (d) imaginary parts of the permittivity found from the fitting parameters. The experimental results are show as symbols and the lines are the fits. Sample a is shown as the circles and solid lines and sample b as the diamonds and dashed lines. . . . .	62
5.4	(a) Time domain and (b) real and (c) imaginary parts of the Fourier transformed frequency domain of the transmission through InSb sample at room temperature. The time domain results are only experimental. In the frequency domain the experimental results are represented as a symbol for every 75 <sup>th</sup> data point and the lines are the fits. (d) Shows the permittivity from the fitted Drude parameters, the solid line is the real part and the dashed imaginary. The inset shows where the real permittivity crosses -1 (shown as the dashed straight line). . . . .	64
5.5	The extracted (a) scattering rate and (b) plasma frequency from the InSb sample at various temperatures. . . . .	65

5.6 A log log plot of the surface plasmon frequency ( $\omega_{sp}$ ) plotted against the scattering rate ( $\gamma$ ) for different semiconductors found in the literature (open shapes) and measured in this paper (filled shapes). The black data points represent room temperature measurements, red ones are above room temperature and blue below. It is discussed in the text that  $\omega_{sp}$  needs to be in the range of typical terahertz time domain spectrometers ( $0.2 \rightarrow 2$  THz, the shaded region) with  $\gamma$  as low as possible. It can therefore be said that InSb is the best candidate for terahertz plasmonic experiments. The bold silicon result is used below for modelling. . . . . 66

5.7 Schematic of the grating profile used for the finite difference time domain modelling. . . . . 68

5.8 Finite difference time domain results for a monograting with a mark to space ratio of 50%. The depth of the grating is varied showing the changing coupling efficiency. The two panels are (a) InSb using the Drude parameters found above, and (b) silicon using Drude parameters from the literature. . . . . 69

5.9 Schematic of the focusing terahertz spectrometer with a third path, allowing the sample to be optically pumped. . . . . 70

5.10 Time domain transmission measurement of InSb at 10 K with no photoexcitation (solid line) and illuminated by a 400 nm pulse (dashed line). 71

5.11 Decay of the induced reduction in the terahertz transmission with time from an optical photoexcitation pulse. Each sub figure shows various temperatures (indicated in the figure) for a single fluence. The fluences are described in the text where (a) shows *iii*, and (b) shows *iv*. . . . . 72

5.12 Three consecutive measurements of the photoexcitation decay using pump fluence *iv* at a temperature of 100 K. The first measurement is the solid line with the first repeat being the dotted line and the second the dashed one. . . . . 73

5.13 Schematic of the conduction and valence bands showing filled electron states as the system is photoexcited. (a) When the system starts without being photoexcited, and (b) where the system has already been photoexcited. . . . . 73

5.14 Decay of the induced reduction in the terahertz transmission with time from an optical photoexcitation pulse. Each sub figure shows various fluences (indicated in each figure) for a single temperature. The temperatures are (a) 50K, and (b) 150K. . . . . 74

5.15	The first part of the decay trace measured at 10 K with pump fluence <i>iii</i> (symbols are the measured values). The rise time can be seen with a fitted Gaussian function (solid line) with a full width half maxima of 27 ps. . . . .	75
5.16	Schematic showing impact ionisation. Here energy from the photoexcited electron <i>a</i> is transferred to electron <i>b</i> as it decays to <i>c</i> , providing energy for <i>b</i> to be excited to <i>d</i> . . . . .	75
6.1	A schematic of the unit cell for pillar localised surface plasmon resonances with example field profiles. . . . .	78
6.2	Reflection spectra for InSb rods (a) connected by an InSb substrate with varying particle heights, $h = 10 \mu\text{m}, 50 \mu\text{m}, 100 \mu\text{m}$ and $150 \mu\text{m}$ , and (b) disconnected square rods ( $h = 10 \mu\text{m}$ ). The dimensions of the rods modelled are length $20 \mu\text{m}$ , and width $10 \mu\text{m}$ , with a separation between the particles of $10 \mu\text{m}$ . The array has a long axis pitch of $60 \mu\text{m}$ and short axis pitch of $20 \mu\text{m}$ . . . . .	79
6.3	Snapped side of InSb wafers at $35^\circ$ where the scale bars are $100 \mu\text{m}$ . (a) An unetched wafer, some stress damage from breaking the sample can be seen, (b) a sample etched using a lactic and nitric acid mix, where the etchant was only incident on the top surface, damage can be seen over $200 \mu\text{m}$ under the surface of the sample, and (c) the material has been etched by $\approx 250 \mu\text{m}$ in nitric acid no damage other than that due to the stress on breaking the sample can be seen. . . . .	81
6.4	The surface of an InSb wafer after etching in nitric acid, (a) an optical microscope image and (b) an SEM image, where the scale bar is $20 \mu\text{m}$ . . . . .	82
6.5	The surface of an InSb wafer after etching in nitric acid with a chromium mask of curved triangles being deposited before etching. This is an optical microscope image, the base to point length of each triangle is around $100 \mu\text{m}$ . . . . .	83
6.6	(a) Schematic view showing the four cuts required to cut a triangular prism particle using a FIB on a flat InSb substrate, the cuts are tapered slightly similar to the shape of the FIB. (b) Three remaining particles on the side of an InSb wafer after teeth have been etched into the edge of the angled side of the wafer before another cut is made to remove the particles from the substrate. (c) An SEM image of a single particle cut from the side of the wafer. . . . .	84



6.7	An optical microscope image showing the positioning of the triangular shaped particles cut using the FIB. The red mark is a positioning point. The cuts into the substrate in the bottom right are where the particles were made. . . . .	85
6.8	(a) A SEM image of the array of triangles cut using a FIB and positioned using a micropositioner. The outer ring is a metallic aperture. (b) The normalised transmission intensity measured through the InSb particles. . . . .	86
6.9	Two regions of the same sample after the lift off procedure. Remaining on the surface should be chromium triangles on a PMMA protective layer on an InSb substrate. The difference between the regions is very visible. The base to point length of the triangles is 100 $\mu\text{m}$ . . . . .	88
6.10	Curling of the chromium layer on the photo resist is observed originating at the edges of some triangles. The point of the stretched pipette is also shown. . . . .	88
6.11	The optical microscope setup used for scraping the chromium mask to clean it. (a) An overview of the microscope, with the camera used shown. (b) The hydraulic micropositioner that was utilised. . . . .	90
6.12	Part of a cleaned array of chromium triangles on a PMMA protective layer on an InSb substrate. . . . .	91
6.13	Photographs of two InSb wafers with PMMA and chromium masks on top. Both show burning from the RIE process. (a) shows the case with the surrounding PMMA and (b) where the surrounding PMMA was first removed. . . . .	91
6.14	Optical microscope images of etched InSb pillars. (a) Side on at an angle of $\approx 75^\circ$ and (b) top down. . . . .	92
6.15	Spectra of field enhancement in between the particles of particle pairs as the separation distance is decreased. These are shown for (a) spherical particles and (b) triangular particles. . . . .	93
6.16	Field plots of the time averaged electric field in a plane cutting through the particles halfway from their base to their top. The spheres have a diameter of 30 $\mu\text{m}$ and the triangles a base to tip length of 30 $\mu\text{m}$ with a thickness of 10 $\mu\text{m}$ . . . . .	93
6.17	Three different methods of altering the sharpness of particles, (a) truncation, (b) rounding and (c) changing the internal angle ( $\alpha$ ). . . . .	94
6.18	Rounded and pointed triangles overlaid showing the difference between the two modelled particle shapes. . . . .	94
6.19	Transmission response for rounded and pointed triangle arrays, the curved triangles are shown as the solid line and the pointed as the dashed. . . . .	95

6.20	Time averaged electric field profiles on a plane cut through the middle of the particle, modelled in an infinite array. The particle thickness is 10 $\mu\text{m}$ , the long axis 61 $\mu\text{m}$ and they are modelled for an array with a pitch of 150 $\mu\text{m}$ . These field plots are for pointed particles as shown, at (a) 0.8 THz, (b) 1.025 THz, and (c) 1.175 THz. . . . .	95
6.21	Time averaged electric field profiles on a plane cut through the middle of the particle, modelled in an infinite array. The particle thickness is 10 $\mu\text{m}$ , the long axis 61 $\mu\text{m}$ and they are modelled for an array with a pitch of 150 $\mu\text{m}$ . These field plots are for curved particles as shown, at (a) 0.85 THz, and (b) 1.125 THz. . . . .	96
6.22	Optical microscopy images of two arrays of (a) triangles and (b) truncated triangles fabricated using the same photolithography mask. . . . .	96
6.23	(a) A schematic of the three triangle types reproduced on the photolithography mask. (b) The transmission through modelled arrays of these three triangles. The sharpest triangles ( $\alpha = 15^\circ$ ) are shown as the solid line, the intermediary particles ( $\alpha = 30^\circ$ ) as the dashed line, and the broad particles ( $\alpha = 60^\circ$ ) as the dotted line. . . . .	96
6.24	Calculated transmission through arrays of InSb triangles, the dashed line is the normal response with the solid line showing the effect of an increase in carrier concentration of $1 \times 10^{16} \text{ cm}^{-3}$ an increase of 50%. . . . .	97
7.1	(a) Scanning electron microscope image of the array of dimples in aluminium, with diameter = 50 $\mu\text{m}$ , depth = 90 $\mu\text{m}$ , and pitch = 90 $\mu\text{m}$ . The sample array is square with the direction of propagation, shown by the arrow, at $45^\circ$ to the lattice vectors. (b) The measured (solid curved line) and analytical modelled (dashed line) dispersion of the terahertz hole array sample. (c) 3D schematic of the unit cell used in numerical modelling. . . . .	101
7.2	Schematic diagrams showing (a) the open hole array sample configuration, (b) the experimental set up, and (c) the unit cell of the experimental sample, with the propagation direction indicated. . . . .	102
7.3	Measured dispersion relations for open and closed metallic hole arrays in the microwave regime, with analytical and finite element method modelling dispersions shown. The field profiles for the symmetric and anti-symmetric surface modes are shown on open ended hole arrays, found using the finite element method. . . . .	110

7.4	The transmission measured across the surface of an array of open ended square holes defined by $d = 9.25\text{mm}$ , $a = 6.96\text{mm}$ , $h = 15\text{mm}$ , and $\epsilon_h = 2.29$ , normalised against the transmission across a flat metal surface.	111
7.5	Surface wave dispersion from the analytical model for open ended hole arrays, (a) where the thickness is varied, and (b) where the surrounding permittivity is asymmetric above and below the sample. . . . .	113
7.6	Dispersion relations for an open ended hole array defined by $a = 6.96\text{mm}$ , $h = 15\text{mm}$ , and $\epsilon_h = 2.29$ when $d = 15\text{mm}$ (solid curved line) and $d = 9.25\text{mm}$ (dashed curved lines). . . . .	115
7.7	(a) Spoof surface mode dispersion relations in the reduced zone representation. For hole arrays defined by $\omega_{co} < \omega_{diff}$ , a number of modes associated with each grating vector are observable in the 1 <sup>st</sup> Brillouin zone. For hole arrays with $\omega_{co} > \omega_{diff}$ (b), only the first two (surface plasmon) modes are defined below cut-off. (c) Transmission as a function of hole height $h$ for an array with dimensions $a = 0.8d$ . One can clearly observe the multimodal transmission, with several peaks in the frequency region between the cut-off frequency (marked by a solid arrow) and $\omega = \omega_{diff}$ . (d) Transmission as a function of hole height $h$ for an array with dimensions $a = 0.4d$ , showing the transmission mediated by the symmetric and antisymmetric surface plasmon modes. The lower panels show transmission spectra at heights indicated by dotted arrows. All calculations are for $\epsilon_h = 1$ . . . . .	119

# Definitions

<i>FEM</i>	Finite element method
<i>FIB</i>	Focussed ion beam
<i>InSb</i>	Indium antimonide
<i>SEM</i>	Scanning electron microscope
<i>SPP</i>	Surface plasmon polariton
<i>TE</i>	Transverse electric (s-polarised)
<i>THz – TDS</i>	Terahertz time domain spectroscopy
<i>TM</i>	Transverse magnetic (p-polarised)
<i>Microwave regime</i>	1 → 200 GHz
<i>Optical/Visible regime</i>	300 → 1000 THz
<i>Terahertz regime</i>	0.2 → 2 THz